THE JOURNAL OF BIOLOGICAL CHEMISTRY
Vol. 279, No. 38, Issue of September 17, pp. 40100–40111, 2004
Printed in U.S.A.

A Model of Myosin V Processivity*

Received for publication, March 8, 2004, and in revised form, June 28, 2004
Published, JBC Papers in Press, July 14, 2004, DOI 10.1074/jbc.M402583200

Steven S. Rosenfeld‡§ and H. Lee Sweeney¶

From the ‡Department of Neurology, University of Alabama, Birmingham, Alabama 35294 and the ¶Department of Physiology, University of Pennsylvania, Philadelphia, Pennsylvania 19104

Cytoplasmic transport is mediated by a group of molecular motors that typically work in isolation, under conditions where they must move their cargos long distances without dissociating from their tracks. This processive behavior requires specific adaptations of motor enzymology to meet these unique physiologic demands. One of these involves the ability of the two heads of a processive motor to communicate their structural states to each other. In this study, we examine a processive motor from the myosin superfamily myosin V. We have measured the kinetics of nucleotide release, of phosphate release, and of the weak-to-strong transition, as this motor interacts with actin, and we have used these studies to develop a model of how myosin V functions as a transport motor. Surprisingly, both heads release phosphate rapidly upon the initial encounter with an actin filament, suggesting that there is little or no intramolecular strain associated with this step. However, ADP release can be affected by both forward and rearward strain, and under steady-state conditions it is essentially prevented in the lead head until the rear head detaches. Many of these features are remarkably like those underlying the processive movement of kinesin on microtubules, supporting our hypothesis that different molecular motors satisfy the requirement for processive movement in similar ways, regardless of their particular family of origin.

Cytoplasmic transport motors are found in both the myosin and kinesin families and typically work in isolation (1, 2). This physiology places a unique requirement on them: they must remain attached to their respective tracks through multiple ATPase cycles. This need for processivity demands that, at any given time, at least one of the two motor-containing "heads" remains strongly attached to its track to prevent the entire motor from prematurely detaching. Such coordination requires appropriate kinetics as well as structural communication between the heads to optimize processive movement.

Myosin V is the first of the myosin superfamily members shown to be processive (3–5, 35). The mechanism underlying its movement has been studied extensively over the past 4 years, and a general picture of how it works has emerged (6). The motor needs to take 36-nm steps along an actin filament to avoid spiraling around the actin filament. Myosin V accomplishes this by possessing large lever arms made up of six "IQ motifs" and their associated light chains (7, 8), and it uses these long lever arms to walk hand over hand along an actin filament for many steps before dissociating. How then is this processive behavior maintained?

The processive behavior of myosin V presumably reflects specific adaptations it has made in its enzymology, which in aggregate facilitates its function as a transport motor. One of these adaptations is the identity of the rate-limiting step of the actin-activated ATPase cycle. The rate-limiting step for most isoforms of myosin II is phosphate release, which insures that the motor spends the majority of its ATPase cycle either detached or weakly bound to actin (*i.e.* low duty ratio). However, for myosin V, the rate-limiting step is ADP release, which allows the myosin to remain strongly bound to actin for the majority of the cycle (*i.e.* high duty ratio). The result of this difference is that myosin V has a duty ratio of ~0.9 at high actin concentrations, compared with duty ratios of 0.03–0.04 for smooth and skeletal muscle myosin II (9). This large duty ratio is a feature that has been thought to be essential for processive, transport motors, because it would reduce the probability of premature dissociation from actin. However, a large duty ratio by itself may not be enough to ensure that myosin V can function properly in its transport role, because we have shown that myosin IIB, a member of the myosin II family designed for tension generation, also has a high duty ratio (10).

In addition to needing large duty ratios, the two heads of processive motors must also communicate their structural states to each other throughout their mechanochemical cycles. This communication is needed to ensure that the two heads do not weakly bind to their track simultaneously, an event that would lead to premature dissociation and that could have dire physiologic consequences. In the case of myosin V, how this allosteric communication is carried out and how it is coupled to the ATPase cycle remain unclear. Three models have recently emerged (5, 11, 12). In the first, the intramolecular strain that develops when both heads are bound to the actin filament mediates this allosteric communication. In this model, *rearward strain* on the *forward head* prevents this motor domain from binding ATP and detaching until the strain is relieved by detachment of the trailing head (11). In the second model, *forward strain* on the *rearward head* accelerates its detachment from actin (5). In both of these models, intramolecular strain plays a central role, much as in the case of microtubule motor kinesin (13), where we have shown that strain accelerates motor dissociation from the trailing head and blocks motor dissociation from the leading head. In the third model, intramolecular strain plays no role at all (12). Rather, strong binding by the rearward head prevents actin binding and phosphate release by the forward head. Processivity in this model would be favored if ATP binding to the rearward head were to lead to rapid and strong binding of the forward head.

Thus, it remains unclear whether strain plays a role at all in the processivity of myosin V, and if so, what effect it has on the

* This work was supported by National Institutes of Health Grants AR048565 (to S. S. R.) and AR35661 (to H. L. S.). The costs of publication of this article were defrayed in part by the payment of page charges. This article must therefore be hereby marked "*advertisement*" in accordance with 18 U.S.C. Section 1734 solely to indicate this fact.

§ To whom correspondence should be addressed: Dept. of Neurology, University of Alabama at Birmingham, FOT 1020, 1530 3rd Ave. S., Birmingham, AL 35294. Tel.: 205-934-0284; Fax: 205-975-7546; E-mail: stevensr@uab.edu.

kinetics of specific transitions in the mechanochemical cycle. Addressing these issues is the focus of this study. Our results show that *both* forward *and* rearward strain can affect the kinetics of crucial structural transitions in the myosin V ATPase cycle. However, under steady-state conditions, it is the effect of rearward strain in retarding ADP release from the forward head that provides the critical coordination for processivity. Our results also show that phosphate release is rapid for both heads and occurs before the heads bind strongly to actin. Taken together these data provide the first evidence that phosphate is released immediately upon myosin V binding to actin and that it occurs prior to formation of a strong binding state and development of intramolecular strain. Our results demonstrate that only the release of ADP is strain-sensitive, ensuring that both heads will be strongly bound to actin once the lead head finds an actin-binding site. Thus the degree of processivity of myosin V is ultimately limited by the rate at which a newly detached head can find an actin binding site. This arrangement ensures that both heads will be strongly bound to actin once the lead head finds an actin-binding site.

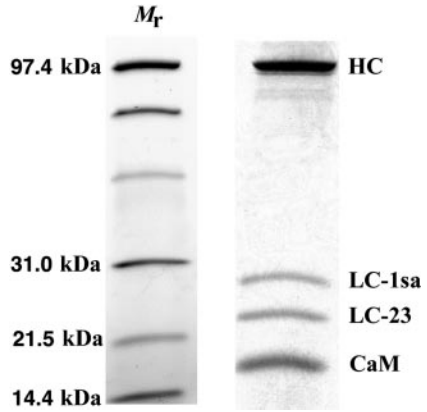

FIG. 1. **Subunit composition of myosin V HMM.** Shown are lanes from Coomassie Blue-stained SDS-PAGE of a myosin V-6IQ HMM construct, co-expressed with calmodulin (*CaM*) and the essential light chains LC-23 and LC-1sa, which produced a product that bound CaM and both ELCs at a ratio of 4:1:1 (CaM:LC-23:LC-1sa). Stoichiometries were determined by laser scanning densitometry of stained gels.

EXPERIMENTAL PROCEDURES

Reagents—The *N*-methylanthraniloyl derivative of 2′deoxy-ADP was synthesized as described previously (24). *N*-1-Pyrenyl iodoacetamide was obtained from Molecular Probes (Portland, OR). Protease inhibitors and chemicals used for buffers were obtained from Sigma. Pre-poured Sephadex G-25 columns (PD10) were obtained from Amersham Biosciences.

Proteins—Actin was prepared from rabbit acetone powder, and labeling at cysteine 374 with *N*-1-pyrenyl iodoacetamide was carried out as described before (14). Phosphate-binding protein was purified from *Escherichia coli* and labeled with MDCC[1] as described (25).

Recombinant Myosin V Expression and Purification—Chicken myosin V cDNA was expressed in two forms. The constructs were based on the previously described two-headed (HMM-like) myosin construct, myosin V-6IQ HMM (7). The construct was used to create either a two-headed (HMM-like) or single-headed (S1-like) construct. This myosin V-6IQ HMM heavy chain was truncated at Glu-1099, to which was added a leucine zipper (GCN4) to ensure dimerization, then followed by a FLAG tag (for purification). For the single-headed (S1-like) construct, the coiled-coil was removed and the heavy chain was truncated at amino acid Lys-910 to create myosin V-6IQ S1. As for the HMM, a FLAG tag was added after Lys-910 to facilitate purification. Recombinant baculoviruses were generated and used for co-expression in SF9 cells with calmodulin and essential light chains (7). Using the methodology detailed previously (26), purified myosin V HMM or S1 protein was obtained. Fig. 1 illustrates an SDS-PAGE of a purified myosin V HMM 6IQ preparation and demonstrates that a typical yield has high purity and minimal evidence of proteolysis. Concentrations of recombinant myosin V preparations were determined with the Bio-Rad protein assay. The reference samples were recombinant myosin V HMM and S1 whose concentrations were determined by absorbance, using calculated extinction coefficients of 540,240 M^{-1} cm^{-1} for HMM and 129,610 M^{-1} cm^{-1} for S1. Complexes of myosin V constructs with 2′dmD were formed by pre-incubating S1 and HMM with a 20-fold molar excess of 2′dmD, followed by gel filtration on pre-poured Sephadex G-25 columns (PD10, Amersham Biosciences) according to the manufacturer's instructions. Fractional labeling of the complexes with 2′dmD was determined by using the extinction coefficient of the fluorescent nucleotide (5700 M^{-1} cm^{-1} at 356 nm (24)) and the measured protein concentration. Ratios of 2′dmD to active site concentration were typically 0.90–0.95.

Kinetic Methodologies—Kinetic measurements were made using an Applied Photophysics SX.18MV stopped-flow spectrophotometer with an instrument dead time of 1.2 ms (27). The excitation and emission wavelengths for monitoring pyrene-labeled actin and MDCC-labeled phosphate-binding protein fluorescence have been described (10). For studies of 2′dmD and 2′dmD·P_i release, mant fluorescence was monitored by both direct excitation (λ_{ex} = 356 nm) and by energy transfer from vicinal tryptophan residues (λ_{ex} = 295 nm), and both methods gave similar results.

RESULTS

Our experimental approach was to compare the kinetics of key steps of the myosin V HMM mechanochemical cycle during the first one to two turnovers to those for an S1 construct, because this would allow us to test the role of internal strain in shaping the kinetics of native myosin V. We also examined the kinetics of several of these steps under steady-state conditions to evaluate the physiologic relevance of our findings.

Actin Binding in the Presence of ADP—Previous studies have noted that dimeric myosin V constructs can aggregate actin filaments under conditions that favor strong binding (28, 29). This effect is presumed to be due to the presence of extended lever arms, which would allow cross-linking of actin filaments and could interfere with spectroscopic measurements. We have addressed this issue by comparing the kinetics of the light scattering increase produced by mixing myosin V S1·ADP with actin to those using HMM·ADP. Fig. 2*A* illustrates a typical light scattering transient, produced by mixing 0.8 μM S1 or HMM (active site concentration) with 6 μM actin in the presence of 1 mM ADP. For S1 (*red*), the transient consisted of a rapid phase (*inset*, *red transient*), sometimes accompanied by a low amplitude (<5% total) slow phase. By contrast, mixing with HMM (*green*) produced two well separated phases. The faster phase (*inset*, *green transient*) constituted ~60% of the total signal amplitude. The slower phase fit a single exponential process (*solid curve*), showed little actin concentration dependence, and measured 0.03–0.05 s^{-1}. We propose that the fast phase for both the HMM and S1 transients represents strong binding of at least one head to actin, whereas the slow phase seen with HMM is due to cross-linking. The HMM-induced cross-linking could be due to one of two possibilities. First, steric constraints on the lever arm could prevent the second head of HMM from binding strongly to the same actin filament. Because of its limited rotational freedom in the ADP state, the second head would only be able to slowly attach to neighboring actin filaments, producing a cross-linked aggregate. This possibility would predict that mixing HMM with pyrene-labeled actin in the presence of ADP should produce a fluorescence *decrease* that is the mirror image of the light scattering transient, *e.g.* two phases of similar amplitude, with the slower phase characterized by a rate constant of 0.03–0.05 s^{-1}. The second possibility is that binding of both heads of

[1] The abbreviations used are: MDCC, *N*-[2-(1-maleimidyl)ethyl]-7-(diethylamino)coumarin-3-carboxamide; mant, *N*-methylanthraniloyl; 2′dmD, 2′-deoxy-mant-ADP; 2′dmT, 2′-deoxy-mant-ATP; PBP, phosphate-binding protein; S1, monomeric construct of myosin V; HMM; dimeric construct of myosin V.

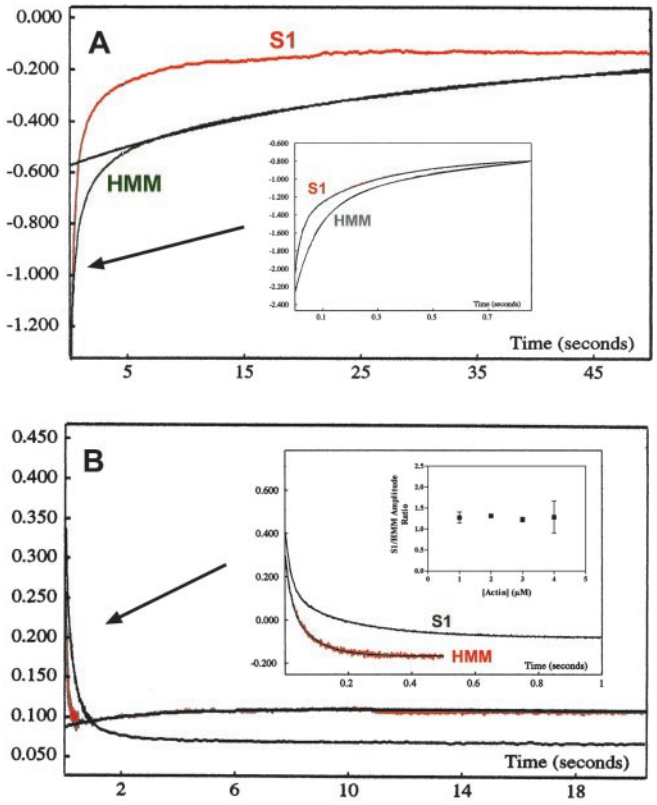

FIG. 2. **Kinetics of myosin V·ADP binding to actin.** *A*, light scattering transients produced by mixing 0.8 μM S1 (*red transient*) or HMM (*green transient*) with 6 μM actin in the presence of 1 mM ADP. For S1, the transient consisted of a rapid phase (*inset*, *red transient*), sometimes accompanied by a low amplitude (<5% total) slow phase. By contrast, mixing with HMM (*green*) produced two well separated phases, and the faster phase (*inset*, *green transient*) constituted ~60% of the total signal amplitude. The amplitude of the faster phase was similar for HMM compared with S1, and in both cases fit a double exponential function (*inset*). The actin concentration dependence defines apparent second order rate constants of ~19 μM^{-1} s^{-1} and 4 μM^{-1} s^{-1} (data not shown). The slower phase fit a single exponential process (*solid curve*), showed little actin concentration dependence, and measured 0.03–0.05 s^{-1}. Conditions: 50 mM KCl, 25 mM HEPES, 2 mM $MgCl_2$, 1 mM EGTA, 1 mM dithiothreitol, pH 7.50, 20 °C. The HMM transient was offset by 0.3 V to make its morphology more readily distinguishable from that for S1. *B*, pyrene fluorescence transient produced by mixing 0.8 μM S1 (*green transient*) or HMM (*red transient*) with 6 μM pyrene-labeled actin (50% labeled) in the presence of 1 mM ADP. For both HMM and S1, the decrease in pyrene fluorescence occurred within 1 s after mixing (*inset*) and could be described by a double exponential function (*solid lines* through the *red* and *green transients*). The actin concentration dependence defines apparent second order rate constants of ~16 μM^{-1} s^{-1} and 0.8 μM^{-1} s^{-1} (*data not shown*). Furthermore, as shown in the inset, the amplitude of the pyrene quenching was nearly identical for HMM and S1 over a range of actin concentrations. For HMM, a low amplitude increase in pyrene fluorescence followed the initial quenching, and it fit a single exponential process at 0.05–0.07 s^{-1} (*solid curve*). Conditions were as in *A*.

HMM to the same actin filament is kinetically favored but leads to a system that is internally strained. In this case, strain could be relieved by release of the forward head (with rate constant of 0.03–0.05 s^{-1}), followed by attachment to a neighboring actin filament. In this scenario, mixing of HMM with pyrene-labeled actin should produce a fast fluorescence decrease that is not followed by a slow phase. Furthermore, this possibility would predict that the amplitude of the fast fluorescence decrease should be the same as that for an equimolar S1 concentration.

Fig. 2*B* illustrates the results of mixing 0.8 μM (active site concentration) S1·ADP (*green*) or HMM·ADP (*red*) with 6 μM pyrene-labeled actin (50% labeled). Strong binding to actin quenches the pyrenyl fluorescence, and for both S1 and HMM, this process (*inset*) is considerably more rapid than cross-linking (Fig. 2*A*). A detailed analysis of the kinetics of this rapid quenching demonstrates biphasic decays for both HMM and S1 (*inset*), with apparent second order rate constants of 16–19 μM^{-1} s^{-1} and 1–4 μM^{-1} s^{-1} (data not shown). More important, the total amplitudes of this pyrene fluorescence transient were nearly identical for equimolar active site concentrations of S1 and HMM preparations (Fig. 2*B*, *inset*). Finally, it should be noted that over the time scale where cross-linking occurs (>2 s after mixing with HMM), no further decrease in pyrene fluorescence was seen in the HMM transients. In fact, a small amplitude rising phase was noted, which fit a single exponential process at 0.05–0.07 s^{-1} (Fig. 2*B*, *solid curve*). As indicated by the discussion above, we interpret these results to mean that, after mixing, both heads of HMM bind relatively rapidly to the same actin filament. We predict that this would generate intramolecular strain, which would be relieved by a slow dissociation of the leading head from one actin filament and its subsequent rebinding to a neighboring filament. Labeling actin with pyrene reduces its affinity for myosin (14). Hence, the combination of rearward strain on the leading head, which would favor its dissociation from actin, with the increased affinity of an ADP-containing head for unlabeled actin, would together lead to rebinding to unlabeled actin subunits on neighboring filaments. This should lead to an overall reduction in pyrene actin subunits with a strongly bound HMM head, because in this experiment, only 50% of the actin subunits were labeled, and this would be manifested by a low amplitude rise in fluorescence at ~0.05 s^{-1}. This prediction is confirmed in Fig. 2*B*.

Actin-activated ADP Release—Because ADP release is rate-limiting in the cycle (9), we investigated the effect of strain on the kinetics of ADP release. This was monitored by mixing a complex of S1·2′dmD or HMM·2′dmD in the stopped flow with actin plus excess nucleotide. Fig. 3*A* illustrates the fluorescence transients produced by mixing a complex of 2 μM (active site concentration) S1·2′dmD (*red*) or HMM·2′dmD (*green*) with 20 μM actin plus 2 mM ADP. For S1, the transient could be fit to a single exponential decay, reflecting dissociation of the bound 2′dmD, and the rate constant of this process varied hyperbolically with actin concentration (Fig. 3*A*, *inset*, *red circles*), defining a maximum rate constant of 15.8 ± 1.6 s^{-1}. This result is very similar to previously reported studies that used mant-ADP, which is a mixture of the 2′ and 3′ isomers (9). By contrast, the corresponding fluorescence transient for HMM was clearly biphasic, and the two phases had similar amplitudes (Fig. 3*B*). Only the faster phase showed a dependence of rate constant on actin concentration (Fig. 3*A*, *inset*, *green boxes*), with an extrapolated maximum of 29.5 ± 3.4 s^{-1}: nearly twice as large as the corresponding value for S1. The slower phase (*inset*, *green triangles*) averaged ≈0.3–0.4 s^{-1} and showed little variation with actin concentration. These results are consistent with the model illustrated in Fig. 3*C*, where the fluorescence of the bound 2′dmD is symbolized by the *magenta* rays emanating from the actin-bound heads. We propose that forward strain on the rear head accelerates ADP release by a factor of approximately two, whereas rearward strain on the forward head markedly slows ADP release, to ≈0.3 s^{-1}. Release of this strain would occur with a slow dissociation of the forward head (at 0.03–0.05 s^{-1}). This would then be rapidly followed by rebinding to a neighboring actin filament, which would likely occur with an altered geometry, one that would be unlikely to generate strain.

We tested this proposal by mixing HMM·2′dmD or S1·2′dmD in the stopped flow with actin plus 2 mM ATP. Because S1

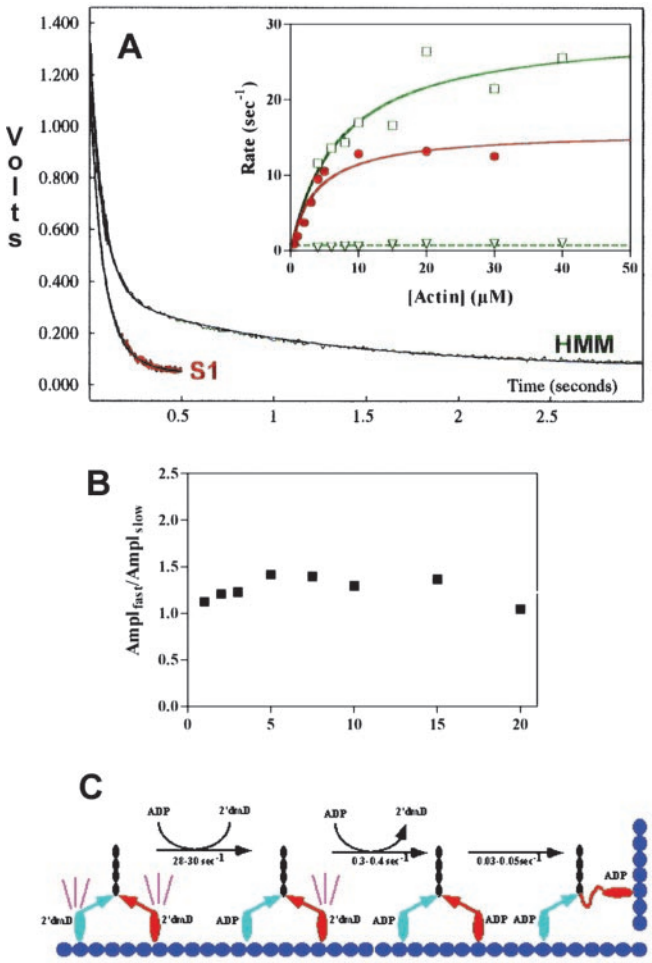

FIG. 3. **Kinetics of actin activated 2′dmD release from myosin V constructs in the presence of 2 mM ADP.** *A*, fluorescence transient produced by mixing a complex of 2 μM (active site concentration) S1·2′dmD (*red jagged curve*) or HMM·2′dmD (*green jagged curve*) with 20 μM actin plus 2 mM ADP. Nucleotide complexes were formed by preincubating S1 and HMM with a 20-fold molar excess of 2′dmD, followed by gel filtration on Sephadex G-25 to remove excess nucleotide. The transient for S1 fit to a single exponential decay, whereas the transient for HMM required a double exponential fit. *Inset*: plot of rate *versus* actin concentration for S1 (*red*) and HMM (*green*). The rate constant of the single phase for S1 fit a rectangular hyperbola, defining a maximum of 15.8 ± 1.6 s^{-1}. Only the faster phase of the HMM transient (*open green boxes*) varied hyperbolically with actin concentration, with an extrapolated maximum of 29.5 ± 3.4 s^{-1}. The slower phase (*open triangles*) showed little actin concentration dependence and averaged 0.3–0.4 s^{-1}. Conditions were as in Fig. 2. *B*, the ratio of the fast phase amplitude of the HMM transient divided by the slow ($Ampl_{fast}$/$Ampl_{slow}$) remained close to 1.0 over a range of actin concentrations. *C*, schematic of the experimental results for HMM. Immediately after mixing, the two heads of HMM (*green* and *magenta*), attach to the actin filament (*blue*) at 36-nm intervals. The fluorescence emission of 2′dmD is enhanced when it is bound to the active site of HMM (symbolized by the *magenta rays* emanating from the motor domains). Release of 2′dmD from the rear head is accelerated 2-fold by the resulting forward strain (symbolized by the *forward pointing green arrow* on the *lever arm*) and produces a 50% reduction in fluorescence. By contrast, rearward strain on the forward head (symbolized by the *rearward pointing magenta arrow* on the *lever arm*) markedly slows 2′dmD release from the forward head, characterized by a rate constant of 0.3–0.4 s^{-1}. Strain is then relieved by an even slower dissociation of the ADP-bound head from one actin filament (at 0.03–0.05 s^{-1}), followed by rapid rebinding to a neighboring filament. Given the altered geometry of binding, this would not be associated with the development of strain and is symbolized by the *serpentine lever arm* in the figure.

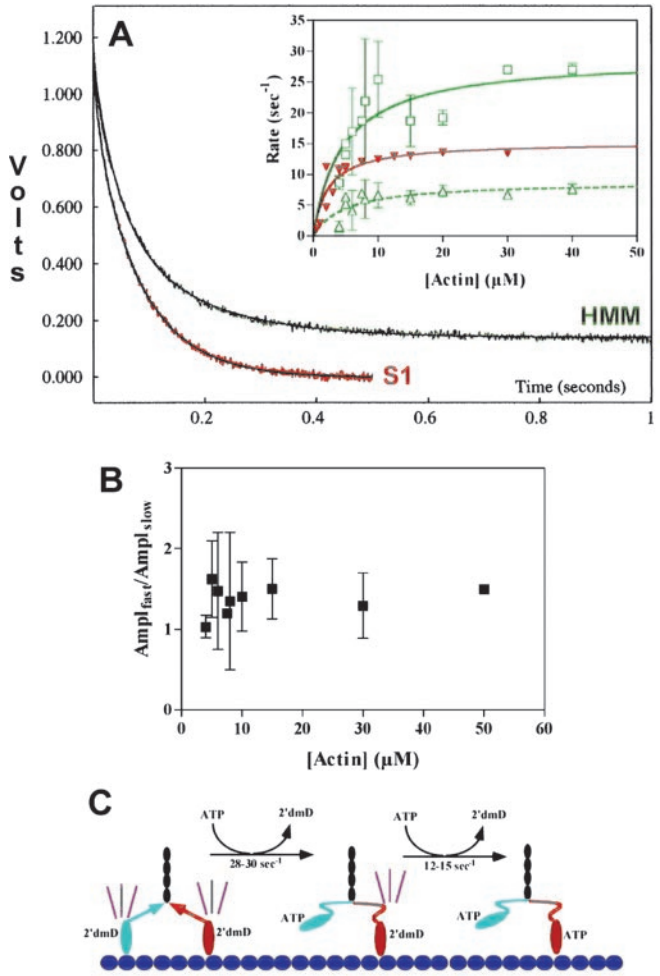

FIG. 4. **Kinetics of actin activated 2′dmD release from myosin V constructs in the presence of 2 mM ATP.** *A*, fluorescence transient produced by mixing a complex of 2 μM (active site concentration) S1·2′dmD (*red jagged curve*) or HMM·2′dmD (*green jagged curve*) with 20 μM actin plus 2 mM ATP. As in Fig. 3, the S1 transient consists of a single phase, whereas that for HMM consists of two phases. The actin concentration dependence of the rate constant for S1 fit a hyperbola (*inset*, *red triangles*) with maximum rate constant of 15.2 ± 1.0 s^{-1}. Both phases of the HMM transient varied hyperbolically with actin concentration (*inset*, *open green boxes* and *open green triangles*), defining maximum rates of 28.9 ± 5.3 s^{-1} and 8.8 ± 1.8 s^{-1}. *B*, as in Fig. 3*B*, the amplitude of the fast phase of the HMM transient is similar to that for the slow, with an average value of $Ampl_{fast}/Ampl_{slow}$ of 1.19 ± 0.24. *C*, schematic of the experimental results for HMM. ADP dissociates from the rear head of a doubly attached, internally strained HMM at the accelerated rate constant of 28–30 s^{-1}. This is rapidly followed by ATP binding and dissociation of the rear head, which relieves the internal strain (symbolized by the *serpentine lever arms*). With strain relieved, ADP can now dissociate from the leading head with a rate constant of 12–16 s^{-1}. Given that these two steps are essentially irreversible, the *observed* rate constant for ADP release from the leading head is predicted to be ≈ [(28 × 12)/(28 + 12)] s^{-1} = 8.4 s^{-1}.

cannot generate internal strain, we would predict that the results with S1 in this experiment should be similar to those for the experiment discussed above. Fig. 4*A* confirms this. The fluorescence transient for S1 (*red*) is well fit by a single exponential decay, and the rate constant of the transient shows nearly an identical hyperbolic dependence on actin concentration (*inset*, *red triangles*, maximum rate constant 15.2 ± 1.0 s^{-1}). Because we are proposing that forward strain accelerates ADP release from the trailing head, we would also expect that the fluorescence transient for HMM should be biphasic and that the maximum rate for the faster phase should be similar to that in Fig. 3*A*. The transient for HMM in this experiment (Fig. 4*A*, *green*) fits a double exponential decay, and the rate constant of the faster phase shows a hyperbolic dependence on actin concentration, which is very similar to that measured in

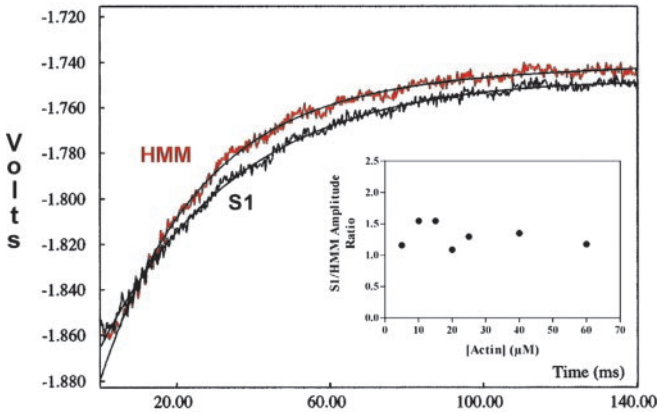

FIG. 5. **Measurement of actin-activated phosphate release from myosin V·ADP·P_i.** 2 μM nucleotide-free construct was mixed with a 10-fold molar excess of ATP, the complex was allowed to age for 1 s to allow population of the myosin V·ADP·P_i state, and it was then mixed with 10 μM actin plus 2 mM ADP. All samples contained 3.5 μM MDCC-PBP. Phosphate release was monitored with MDCC-PBP, and the fluorescence increase fit a single exponential process for both S1 (*green*) and HMM (*red*), described by rates of 23.1 and 42.0 s^{-1}, respectively. *Inset*: ratio of amplitudes of the single exponential fit were plotted as S1·HMM amplitude ratio *versus* actin concentration. The mean amplitude ratio over this range of actin concentrations was 1.28 ± 0.18.

the presence of ADP (*inset*, *green boxes*, maximum rate constant 28.9 ± 5.3 s^{-1}). By contrast, the rate constant of the second phase for the HMM transient in this experiment was considerably faster, with a maximum of 8.8 ± 1.8 s^{-1} (*inset*, *green triangles*). As in the case of Fig. 3, the relative amplitudes of the two phases for HMM were similar (Fig. 4*B*). These results are consistent with the scheme depicted in Fig. 4*C*. Although excess ADP would keep HMM strongly bound and under strain, and while strain would inhibit 2′dmD release from the leading head, excess ATP would bind to the trailing head once it had released its 2′dmD. This would dissociate the trailing head, relieve the internal strain (symbolized by a serpentine regulatory domain) and allow 2′dmD to dissociate from the leading head. A maximum rate constant of 8.8 ± 1.8 s^{-1} (Fig. 4*A*, *inset*, *green triangles*) would be consistent with the model depicted in Fig. 4*C* if release of 2′dmD from the trailing head were immediately followed by ATP binding and dissociation from actin, allowing 2′dmD to release from the leading head at a rate defined by our studies with S1 (12–15 s^{-1}; Ref. 9 and Fig. 4*A*).

Kinetics of Phosphate and Product Release—We measured the kinetics of actin-activated phosphate release from myosin V S1 and HMM at equal active site concentrations in a sequential mixing experiment. Nucleotide-free S1 or HMM was mixed with a 10-fold molar excess of ATP, the complex was allowed to age for 1 s to allow population of the myosin V·ADP·P_i state, and it was then mixed with varying concentrations of actin plus 2 mM ADP. Phosphate release was monitored with MDCC-labeled phosphate-binding protein (MDCC-PBP), as previously described (10), with a MDCC-PBP·myosin concentration ratio of 7:1 after the second mix. Fig. 5 illustrates an example of the resulting fluorescence transients for HMM (*red*) and S1 (*black*) at final active site concentrations of 0.5 μM and at a final actin concentration of 5 μM. For both constructs, the fluorescence fit a single exponential process (*solid curves* in Fig. 5). The S1·HMM amplitude ratio averaged 1.28 ± 0.18 over a range of actin concentrations (Fig. 5, *inset*). Finally, the rates of phosphate release from both S1 (Fig. 6*B*, *closed red circles*) and HMM (Fig. 7*B*, *closed red circles*) showed a similar hyperbolic dependence on actin concentration, defining maximum rates of 198 ± 18 s^{-1} for S1 and 228 ± 32 s^{-1} for HMM.

We next examined the kinetics of product release in the following experiment. S1 was mixed with a 10-fold molar excess of 2′dmT in a sequential stopped flow, the sample was aged for 1 s to allow formation of an S1·2′dmD·P_i intermediate, and the complex was then mixed with actin plus 2 mM ATP. Because phosphate release from S1 is very rapid, we would expect that the resulting fluorescence decay, reflecting mant-ADP release, should be monophasic. Furthermore, it should be identical to the *red transient* depicted in Fig. 4*A* and have the same rate constant dependence on actin concentration as seen in the *inset* of that figure. In fact, we observed a more complex fluorescence decay, which is illustrated in Fig. 6*A* (*red transient*). The decay was biphasic and fit a double exponential function (*solid line*). The rate constant for the faster phase (Fig. 6*B*, *closed blue boxes*) varied hyperbolically with actin concentration (*solid blue curve*), defining a maximum rate constant of 200 ± 75 s^{-1}. Fig. 6*B* also shows that this process and phosphate release (*red circles*) occur with similar rate constants over a wide range of actin concentrations. The rate constant of the slower phase (*open blue boxes*) showed little variation with actin concentration, and averaged 10–14 s^{-1}. This is very close to the maximum rate constant for 2′dmD release from S1 (Figs. 3*A* and 4*A*), and we propose that it reflects the release of 2′dmD in this experiment as well. The faster phase could be due to one of two possibilities: a conformational change in the catalytic site that precedes 2′dmD release and that occurs with either the weak-to-strong transition or phosphate release, or rapid release of 2′dmD from a sub-population of S1 molecules that are damaged. To distinguish between these two possibilities, we performed the following experiments. First, S1 was mixed in a sequential mixer with a slight molar excess of unlabeled ATP, aged for 1 s, and then mixed with actin plus 200 μM 2′-deoxy-mant-ATP. The mant fluorescence was monitored by energy transfer from vicinal tryptophan residues. If a subpopulation of damaged S1 molecules released nucleotide rapidly, we would expect a biphasic fluorescence increase that would be the mirror image of the *red fluorescence transient* in Fig. 6*A*. Conversely, if ADP release were preceded by a rapid conformational change, we would expect to see only a single phase in the fluorescence increase, reflecting ADP release at 12–15 s^{-1}, and the rate constant would vary little with actin concentration. The *inset* in Fig. 6*A* demonstrates an example of the resulting fluorescence transient. The fluorescence increase fits a single exponential process with little actin concentration dependence. Its mean value of 10.2 ± 1.6 s^{-1} (Fig. 6*B*, *solid green circles*) is nearly identical to that for ADP release. Note that, at a final concentration of 100 μM in this experiment, 2′dmT would be expected to bind to a vacant catalytic site of acto-S1 with a rate constant of ~100 s^{-1} (9). Thus, our finding of a monophasic rise in fluorescence in this experiment is not due to a limitation in 2′dmT concentration.

If the initial rapid fluorescence drop represents a conformational change that accompanies phosphate release, then it follows that the fluorescence intensity of myosin V·2′dmD·P_i should be higher than that for myosin V·2′dmD. We can therefore make one further prediction: mixing S1 with a sub-stoichiometric amount of 2′dmT should produce an initial rise in fluorescence that is larger than that seen with an equivalent amount of 2′dmD. Because phosphate release would be very slow in the absence of actin (0.02 s^{-1} (9)), this initial rise should then be followed by a slow decay as the S1·2′dmD·P_i is converted to S1·2′dmD. Fig. 6*C* compares fluorescence transients produced by mixing 7.5 μM S1 with 5 μM 2′dmT and 5 μM 2′dmD. Consistent with the prediction, the initial rise produced by mixing with 2′dmT (*red transient*) is followed by a slow decay with a rate constant of 0.011 s^{-1} (*solid blue curve*), to a

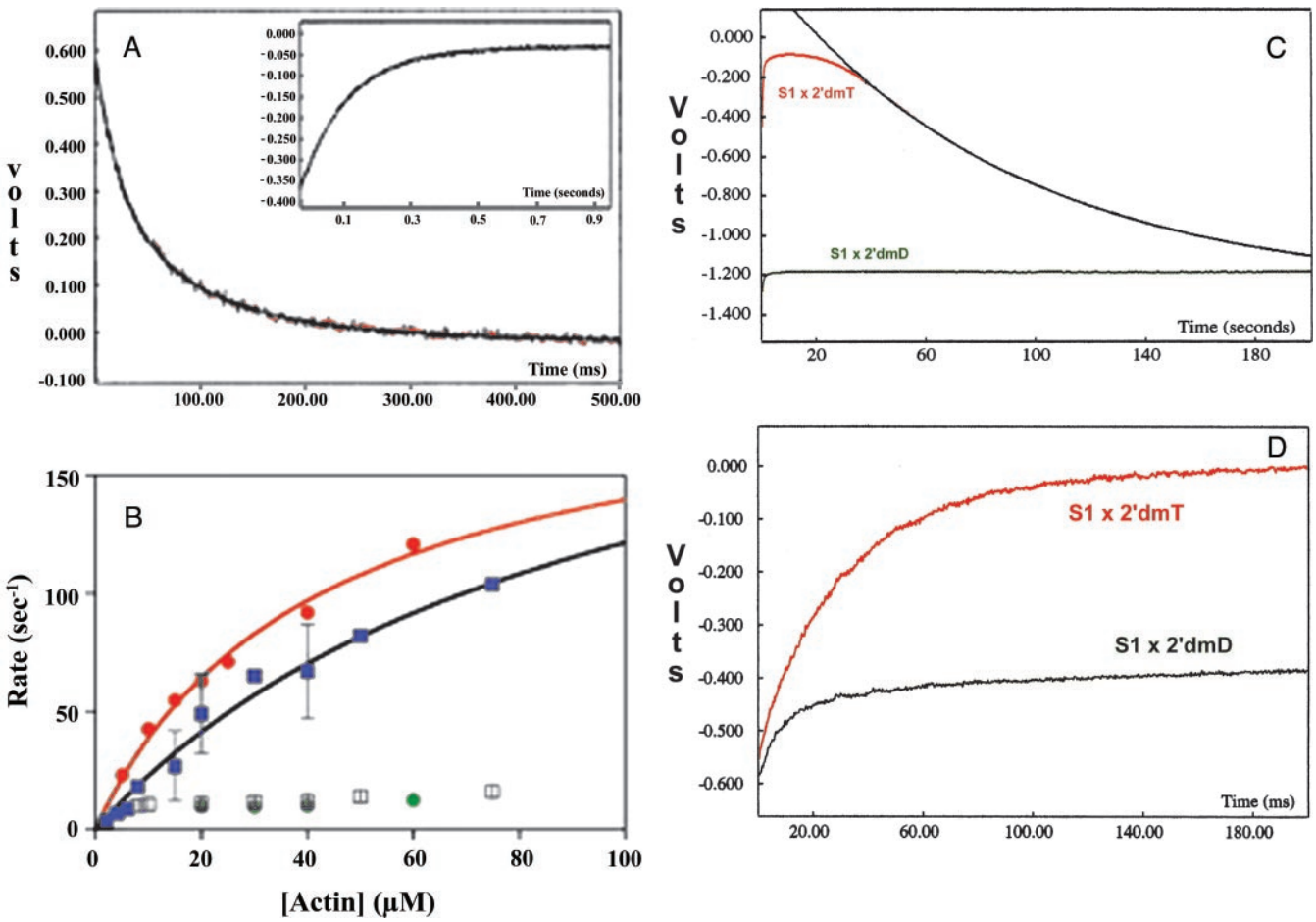

FIG. 6. **Kinetics of product release for S1.** *A*, fluorescence transient produced by mixing 4 μM S1·2′dmD·P_i with 20 μM actin plus 2 mM ATP. The resulting fluorescence decrease (*jagged red curve*) fit a double exponential function (*solid black line*). *Inset*: mixing 2 μM S1 with a 20 μM unlabeled ATP, followed by 20 μM actin plus 200 μM 2′dmT produced a monophasic rise in fluorescence. *B*, plot of rate *versus* actin concentration for product release reactions. S1 was mixed sequentially with a 10-fold excess of 2′dmT and then with actin plus 2 mM ATP, and the rates of both phases (*closed blue boxes* and *open blue boxes*) are plotted *versus* actin concentration. The rate constant of the faster phase varied hyperbolically with actin concentration with maximum rate of 200 ± 75 s^{-1}, whereas the slower phase showed little actin concentration dependence and ranged between 10 and 14 s^{-1}. The rate constant of the fluorescence rise illustrated in the inset (*solid green circles*) varied little with actin concentration, and its mean value is 10.2 ± 1.6 s^{-1}. The rate of phosphate release, measured with MDCC-labeled phosphate binding protein, *versus* actin concentration is also shown (*solid red circles*), and a hyperbolic fit defines a maximum rate constant of 198 ± 18 s^{-1}. *C*, fluorescence transients produced by mixing 7.5 μM nucleotide-free myosin V S1 in the stopped flow with 5 μM 2′dmT (*red transient*) or 2′dmD (*green transient*). For 2′dmT, an initial rapid rise in fluorescence is followed by a slow decay with rate constant of 0.11 s^{-1} (*solid blue curve*), whereas for 2′dmD, only a rapid rising phase is seen. Note that the final voltage for the transient with 2′dmT is nearly identical to that for 2′dmD. *D*, fluorescence transients produced by mixing 7.5 μM nucleotide-free myosin V S1 in the stopped flow with 37.5 μM 2′dmT (*red transient*) or 2′dmD (*green transient*). The amplitude of the transient with 2′dmT is 2.4-fold larger than that for 2′dmD.

final voltage nearly identical to that seen by mixing with 2′dmD (*green transient*). Finally, as predicted, mixing 7.5 μM S1 with a 5-fold molar excess of 2′dmT produces a transient whose amplitude is 2.4-fold larger than that seen with an equivalent concentration of 2′dmD (Fig. 6*D*).

Our results would predict that the corresponding experiment with HMM should produce a fluorescence decrease consisting of *three* phases. The first would be associated with the conformational changes that also lead to phosphate release and would be rapid. The second would be due to release of 2′dmD from the trailing head at 28–30 s^{-1} (Figs. 3*A* and 4*A*), and the third would be due to release of 2′dmD from the leading head at 8–9 s^{-1} (Fig. 4*A*). Furthermore, the amplitudes of the slower two phases should be equal to each other, because each phase represents 2′dmD release from an active site. Fig. 7*A* illustrates the fluorescence transient produced by mixing 4 μM HMM·2′dmD·P_i with 40 μM actin plus 2 mM ATP. The transient (*red jagged curve*) can be fit to three exponential terms (*solid black curve*). Furthermore, the two slower phases demonstrated similar amplitudes over a range of actin concentrations (Fig. 7*B*). Fig. 7*C* demonstrates that the fastest phase (*solid blue boxes*) varies hyperbolically with actin concentration, defining a maximum rate constant of 165.7 ± 28.6 s^{-1}. Furthermore, over the range of actin concentrations tested, the rate constant for this phase is similar to that for phosphate release (*solid red circles*). The second phase (*open blue boxes*) also varies hyperbolically with actin concentration, and this dependence extrapolates to a maximum rate constant of 26.6 ± 4.7 s^{-1}. Finally, the third phase (*solid blue circles*) shows little actin concentration dependence and averages 9.4 ± 1.1 s^{-1}. As a further test of these results, we mixed HMM with a slight molar excess of unlabeled ATP and then with actin plus 200 μM 2′dmT, as was discussed above for S1. The *inset* in Fig. 7*A* demonstrates that the fluorescence transient resulting from mixing HMM·ADP·P_i with 100 μM actin plus 200 μM 2′dmT is clearly biphasic and could be fit to two exponential terms with rate constants of 22.5 and 5.9 s^{-1}.

The Weak-to-Strong Transition—We utilized the quenching of pyrene-labeled actin (14) to monitor the kinetics of the weak-to-strong transition in myosin V by means of the following

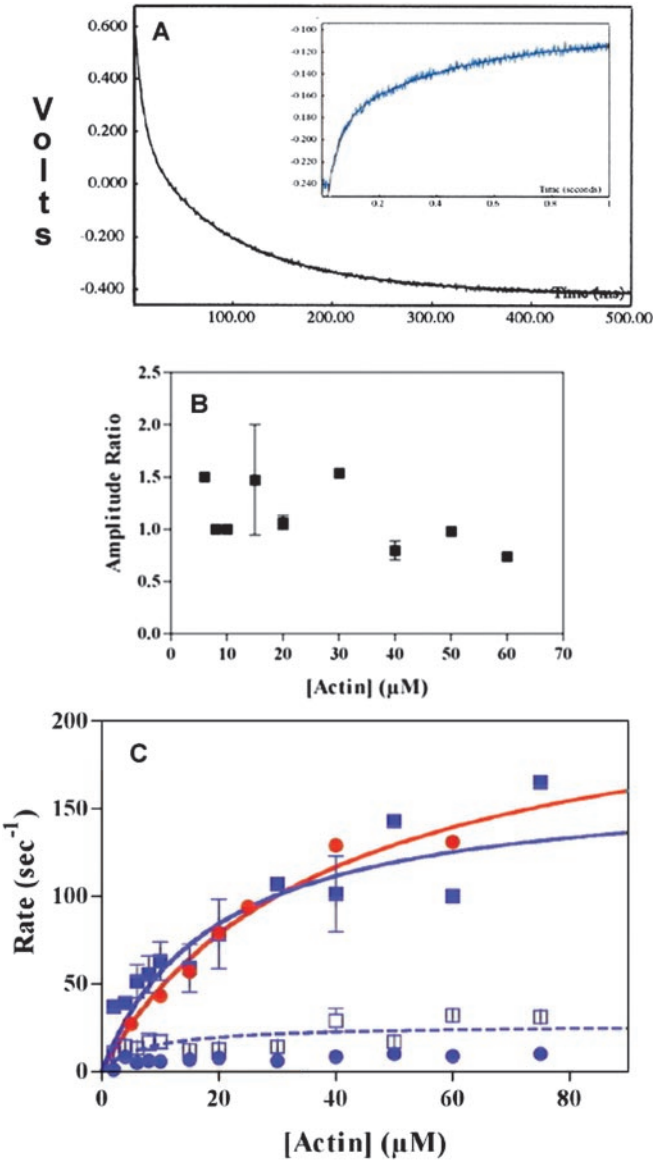

FIG. 7. **Kinetics of product release for HMM.** *A*, fluorescence transient produced by mixing 2 μM HMM·2′dmD·P_i with 20 μM actin plus 2 mM ATP. The resulting fluorescence decrease (*jagged red curve*) could be fit a three exponential decay (*solid black line*). *Inset*: mixing 2 μM HMM with a 200 μM unlabeled ATP, followed by 100 μM actin plus 200 μM 2′dmT produced a biphasic rise in fluorescence with rates of 22.5 and 5.9 s^{-1}. *B*, a plot of the ratio of the amplitude of the two slower phases *versus* actin concentration, demonstrating a similarity in the amplitudes of these two phases over a range of actin concentrations. *C*, the rates of the three phases produced by mixing HMM·2′dmD·P_i with actin plus 2 mM ATP are plotted as a function of actin concentration. The rates of the first two phases (*closed blue boxes* and *open blue boxes*) varied hyperbolically with actin concentration, defining maximum rate constants of 165.7 ± 28.6 s^{-1} and 26.6 ± 4.7 s^{-1}, respectively. The slowest phase showed little actin concentration dependence, and averaged 9.4 ± 1.1 s^{-1}. The rate constant for phosphate release, measured with MDCC-labeled phosphate binding protein, *versus* actin concentration is also shown (*solid red circles*), and a hyperbolic fit defines a maximum rate constant of 228 ± 32 s^{-1}.

experiment. HMM or S1 at equimolar active site concentrations was mixed with a 5-fold molar excess of ATP in a sequential stopped flow as described above. The mixture was allowed to age for 1 s to allow population of the myosin V·ADP·P_i state, and it was then mixed with a 5-fold molar excess of pyrene-labeled actin plus 2 mM ADP. The decrease in fluorescence fit a single exponential decay for both HMM and S1 (data not shown). The rate constant for this process varied hyperbolically

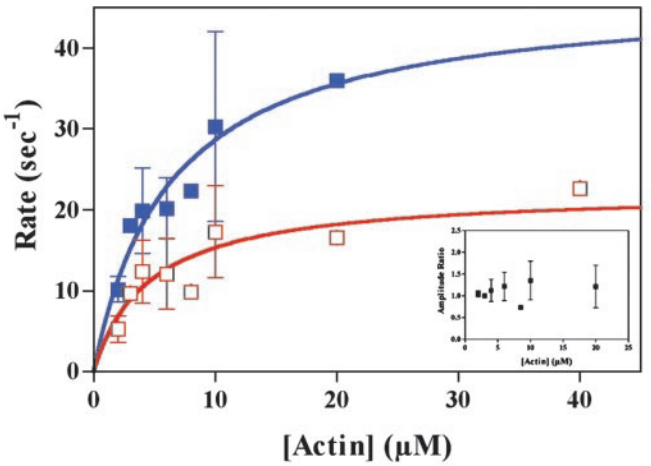

FIG. 8. **Kinetics of formation of a strong binding state.** HMM or S1 was mixed with a 5-fold molar excess of ATP, the mixture was allowed to age for 1 s, and it was then mixed with a 5-fold molar excess of pyrene-labeled actin plus 2 mM ADP. The resulting decrease in fluorescence fit a single exponential decay for both HMM and S1 (*data not shown*). The rate constant for this process varied hyperbolically with actin concentration for both HMM (*solid blue boxes*) and S1. *Inset*: the S1·HMM amplitude ratio for the pyrene actin signal averaged 1.13 ± 0.40 over a range of actin concentrations.

with actin concentration (Fig. 8) for both HMM (*solid blue boxes*) and S1 (*open red boxes*), defining maximum rates of 46.9 ± 13.3 s^{-1} and 22.4 ± 4.0 s^{-1}, respectively. The S1·HMM amplitude ratio averaged 1.13 ± 0.40 over a range of actin concentrations (Fig. 8, *inset*).

Product Release and Strong Binding in the Steady State—We have demonstrated that ADP release by the rear head is accelerated 2-fold during the first turnover of a processive run. Furthermore, our results with the kinetics of the weak-to-strong transition argue that, once the trailing head is released, it swings forward and reattaches to the actin filament very rapidly. This would predict that, in the steady state, product should be released at 28–30 s^{-1}. However, a different result would be expected if, under steady-state conditions, strain only affected ADP release from the leading head. In this situation, ADP release from the trailing head would occur at the unstrained rate of 12–15 s^{-1}, which would produce an overall rate for product release from the two heads of 8–10 s^{-1}. We evaluated this issue by measuring the rate of mant nucleotide release in the following sequential mixing experiment. A complex of 2 μM HMM plus 15 μM actin was mixed with 100 μM 2′dmT. The mixture was incubated for 2 s to achieve a steady-state distribution, and it was subsequently mixed with 4 mM ATP. We would predict the resulting transient to consist of a small amplitude rapid decrease in fluorescence, representing phosphate release by a small fraction of heads, followed by a single phase of further fluorescence decrease, due to product release from the two heads. Fig. 9*A* (*red transient*) depicts the results for HMM, confirming a small amplitude (9% of the total) decrease at 47 s^{-1}, consistent with the rate of phosphate release at this actin concentration (Fig. 7*B*), followed by the major phase characterized by a rate constant of 8.8 s^{-1}. For S1 (*green transient*), a similar biphasic transient was observed with rate constants of 54 s^{-1} (12% of total signal amplitude) and 12.2 s^{-1}. As with HMM, the rate constant for the faster phase for S1 was consistent with that for phosphate release (Fig. 6*B*).

Our argument that rearward strain on the leading head controls processivity in myosin V predicts that, under steady-state conditions, an appreciable fraction of the forward heads is strongly bound, and presumably, experiencing rearward

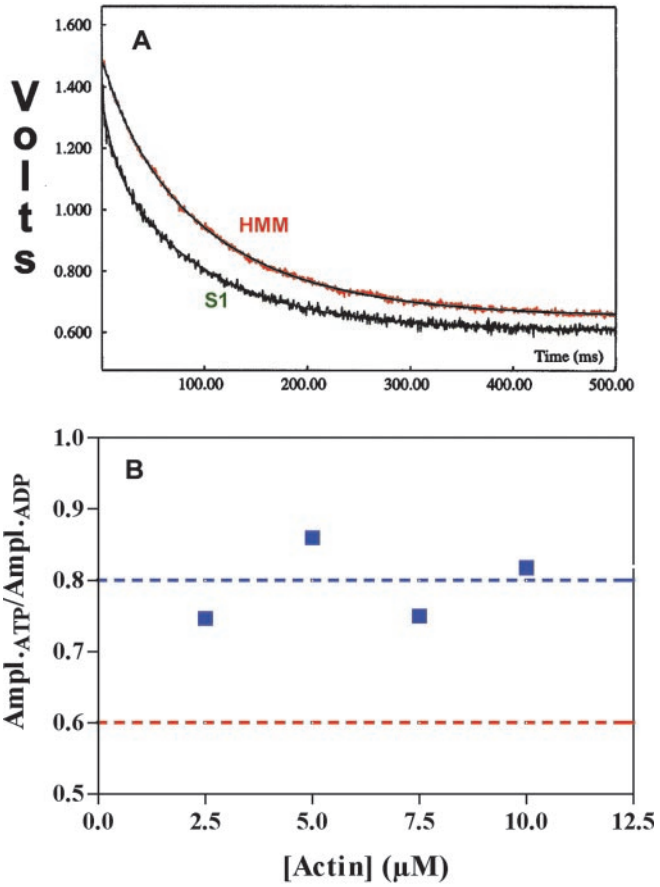

FIG. 9. **Product release and strong binding in the steady state.** *A*, a complex of 2 μM HMM plus 15 μM actin was mixed with 100 μM 2′dmT. The mixture was incubated for 2 s to achieve a steady-state distribution, and it was subsequently mixed with 4 mM ATP. We would predict the resulting transient to consist of a small amplitude rapid decrease in fluorescence, representing phosphate release by a small fraction of heads, followed by a single phase of further fluorescence decrease, due to product release from the two heads. The results for HMM (*red transient*) demonstrate a small amplitude (9% of the total) fluorescence decrease with rate constant of 47 s^{-1}, consistent with the rate of phosphate release at this actin concentration (Fig. 7*B*), followed by the major phase characterized by a rate constant of 8.8 s^{-1}. For S1 (*green transient*), a similar biphasic transient was observed with rate constants of 54 s^{-1} (12% of total signal amplitude) and 12.2 s^{-1}. As with HMM, the rate constant for the faster phase for S1 was consistent with that for phosphate release (Fig. 6*B*). *B*, HMM was mixed with a 5-fold molar excess of pyrene-labeled actin in the presence of 2 mM ATP (final concentration), and the final amplitude of the fluorescence quenching was compared with a similar experiment in the presence of 2 mM ADP. The ratio of the signal amplitudes under the two conditions ($Ampl._{ATP}$/$Ampl._{ADP}$) is plotted *versus* actin concentration in the figure. This demonstrates a mean amplitude ratio of 0.81 ± 0.04. The *blue dotted line* represents the expected value if all of the trailing heads and 50% of the leading heads are strongly bound in the steady state, whereas the *red dotted line* represents the expected value if only the trailing heads were strongly bound in the steady state.

strain. We examined this by mixing in the stopped flow myosin V HMM with a 5-fold molar excess of pyrene-labeled actin in the presence of 2 mM ATP (final concentration) and measuring the final level of fluorescence after 2 s (prior to any appreciable cross-linking). Results were compared with a similar experiment in the presence of 2 mM ADP, and the ratio of the signal amplitudes under the two conditions is plotted *versus* actin concentration in Fig. 9*B*. This demonstrates a mean amplitude ratio of 0.81 ± 0.04. Given the amplitude data in Fig. 8, this implies that all of the trailing heads and ~50% of the leading heads are strongly bound to actin during a processive run. This result effectively eliminates models of myosin V processivity that do not include an intermediate in which both heads are strongly attached (12).

DISCUSSION

The purpose of these studies was to determine how mechanical strain influences the enzymology of myosin V and how strain-mediated effects lead to processivity. Our approach was to compare the kinetics of the weak-to-strong transition, phosphate release, and ADP release for an S1 construct, which cannot generate internal strain, to those for an HMM construct, which can.

Actin Binding in the Presence of ADP—Although our HMM preparations were able to cross-link actin filaments in the presence of ADP, our results with light scattering and pyrene actin fluorescence quenching clearly show that this cross-linking reaction is slow, becoming apparent only after ~5 s after mixing, and it is well resolved kinetically from the initial strong binding of the heads to actin. Furthermore, our results with S1 and HMM (Fig. 2*B*) are consistent with a model in which both heads of HMM initially bind to the same actin filament to generate an internally strained system. In this model (*see below*) ADP release from the lead head would be markedly slowed by rearward strain. We do find that the initial rapid strong binding of HMM and S1 to actin in the presence of ADP is biphasic, with apparent second order rate constants similar to those published previously for myosin V S1 and myosin V S1·ADP (9). We believe that this biphasic behavior is a result of the lower temperature used in our current studies (20 °C), which enhances formation of a rigor conformation even in the presence of ADP.[2] Nevertheless, our results do clearly indicate that, for kinetic processes that are completed in <2–3 s, cross-linking of actin by HMM should not produce confounding effects.

The Strain-sensitive Step—If intramolecular strain mediates the inter-head communication needed to prevent premature dissociation, it must work by altering the kinetics of one or more steps in the mechanochemical cycle. One of these steps must be rate-limiting, which for myosin V is ADP dissociation (9). Our results support this conclusion, because they show that ADP release is strain-dependent under conditions where both heads initially bind to actin. Under these conditions, we found that, although *forward* strain accelerates ADP release by a factor of ~2.0, *rearward* strain slows ADP release at least 50-fold (Figs. 3 and 4). Thus, the major effect of strain appears to be on the leading head. This conclusion raises a question about the physiologic relevance of strain-accelerated ADP release from the trailing head. We examined this issue by measuring the release of 2′dmD under steady-state conditions (Fig. 9*A*) and found that, during the course of a processive run, strain only affects ADP release from the leading head. These results imply that gating of two-headed myosin V during steady-state processive movement is achieved by preventing the ADP-releasing isomerization of the lead head, rather than by accelerating the ADP-releasing isomerization of the rear head. This difference in the ADP release rates from the rear head in the steady state *versus* the initial encounter implies that the geometry of the initial encounter is different from that of subsequent encounters. This is reasonable, because under the conditions of most of the experiments in this study (Figs. 3–8), both heads are in the same state (*e.g.* ADP-P_i or ADP) prior to the initial encounter with actin. By contrast, during processive movement, the two heads would generally be in different enzymatic states to ensure that at least one head is strongly bound to actin at all times.

A somewhat different conclusion was reached in previous

[2] S. S. Rosenfeld and H. L. Sweeney, unpublished observation.

optical trap studies (5), which reported an ~1.5-fold acceleration of ADP release from the rear head by the lead head during processive stepping. However, this conclusion was based on comparisons of single encounters of two-headed myosin V molecules with encounters during processive runs. What was observed was that the lifetime of the state preceding ADP release was ~107 ms in a single encounter case, *versus* 67–75 ms during a processive run. It was concluded that ADP release from the rear head was faster during processive movement than during a single-headed encounter. However, our results suggest a different interpretation. A lifetime of 67- to 75-ms duration would correspond to an ADP dissociation rate of 13–15 s^{-1}, which is what we observed for an S1 construct that cannot generate internal strain. We suggest instead that the event of 107-ms duration that these authors noted was due to a two-headed single encounter, and not simply interaction by one head, as argued in that study (5). If the HMM single encounter was two-headed, as we have concluded from our data in this study, then its duration at saturating ATP concentrations would be ≈33 ms (30 s^{-1} ADP off rate from rear head) plus ≈77 ms (13 s^{-1} ADP off rate from the lead head) = ≈110 ms, which is in very good agreement with the duration measured by Veigel *et al.* (5). Thus, we believe that the data of Veigel *et al.* is in fact consistent with our conclusion, that a modest acceleration of ADP release from the rearward head only occurs during an initial two-headed encounter and is not present during a processive run.

Clearly the geometry of this initial encounter must be different from that of subsequent encounters, because both heads begin in pre-power stroke states. The data of Veigel *et al.* (5) suggest that the heads are binding to actin monomers that are ~25 nm apart and that this geometry allows the lead head to strain the rear head in a manner that accelerates ADP release. When the processive behavior of a myosin V with a short (4IQ) lever arm was characterized, the short lever arms constrained the lead head to take 24-nm steps during steady-state movement (7). Intriguingly, the steady-state ADP release rate from the rear head was accelerated about 2-fold compared with wild-type myosin V. One way to explain these findings is to argue that ADP release is accelerated from the rearward head by forward strain, but only when this strain has a torsional component, *e.g.* a component orthogonal to the long actin filament axis. Because myosin V traffics through a densely branching and intersecting actin meshwork within the cell, it may be advantageous to have a mechanism that accelerates ADP release from a rear head if the lead head side-steps onto a different actin filament. Under these conditions, the lead head might not experience any appreciable rearward strain, which would allow a simultaneous release of ADP from both heads, thus terminating a processive run. Acceleration of ADP release from the rear head under these conditions might therefore help prevent this premature run termination.

Phosphate Release and Movement of Switch I—Phosphate cannot be released from myosin in the pre-power stroke state that initially binds weakly to actin, because it is surrounded by the elements of the nucleotide binding pocket, which include the P loop, switch I, and switch II (15–17). Thus, the structural changes accompanying binding to actin must open an escape route, referred to as a "back door," to enable the release of phosphate (18). Although the mechanism for this process has not been defined, our results with the fluorescent nucleotide 2′-deoxy-mant-ATP (Figs. 6 and 7) provide insight into what these structural changes might be. Mixing a complex of S1·2′dmD·P_i or HMM·2′dmD·P_i with actin produced an initial rapid drop in mant fluorescence, which we have shown is due to a change in the environment of mant nucleotide while it is still bound to the active site. This fluorescence transition provides the first experimental evidence that a conformational change in the nucleotide-binding pocket accompanies phosphate release. This conformational change follows the initial weak binding to actin, hence, the free energy that drives this process must be derived from actin binding, and this in turn argues that phosphate release is accompanied by an increase in actin affinity. It should be noted that this increase in affinity would not constitute "strong" binding, because it precedes the step in the cycle that quenches the pyrene fluorophor on actin (Fig. 8). Insights into the structural basis for this change come from crystallographic studies of *Dictyostelium* myosin II complexed with 2′dmD and of nucleotide-free myosin V (17, 19). These studies have shown that the mant fluorophor in complexes of *Dictyostelium* myosin II:2′dmD is within 2–3 Å of asparagine 214 and aspartate 215, two polar residues located in switch I. If opening of the phosphate back door and movement of the upper 50 kDa subdomain were coupled to movement of switch I, and if this movement of switch I brought these two polar residues in closer proximity to the mant fluorophor, then phosphate release would be accompanied by a quenching of the mant emission, a prediction supported by the data in Figs. 6 and 7. The fact that phosphate release from both heads is rapid implies that intramolecular strain does not affect this step. One possibility is that the conformational changes that lead to phosphate release do not cause the lever arm to swing. Although the mant signal discussed above could indicate an involvement of switch I, the structural changes responsible for phosphate release remain unclear and will require further study.

The Weak-to-Strong Transition—We have shown that the quenching of the pyrene fluorophor on actin (Fig. 8) occurs after phosphate release for both monomeric and dimeric myosin V constructs. Furthermore, we argue, based on the data in Figs. 6 and 7, that phosphate release produces an increase in actin affinity that precedes the pyrene-quenching step. Combining this information allows us to propose a pathway for the myosin V mechanochemical cycle as in Reaction 1,

$$A + (M{\cdot}D{\cdot}P_i)^{**}_{weak} \leftrightarrow A{\cdot}(M{\cdot}D{\cdot}P_i)^{**}_{weak}$$
$$\rightarrow A{\cdot}(M{\cdot}D)^{*}_{intermediate} \leftrightarrow A{\cdot}(M{\cdot}D)^{*}_{strong} \leftrightarrow A{\cdot}M_{strong}$$

REACTION 1

where the asterisks refer to states of enhanced mant fluorescence emission, the actin binding affinity is indicated by subscripts, and where *A* is actin, *M* is myosin V, *D* is ADP, and P_i is inorganic phosphate. Conformational changes that occur in the catalytic site and open the phosphate back door quench the mant fluorescence and allow phosphate to be released. We propose that formation of the initially weak actin bond releases sufficient free energy to drive a change in the conformation of the catalytic site. This would be associated with an increase in actin affinity to an "intermediate" level, one that does not quench the pyrene fluorophor. This is indicated in the reaction pathway by the *intermediate* subscript. This step would then be followed by formation of a strong binding conformation, with its associated quenching of the pyrene fluorophor, followed in turn by release of 2′dmD. As in the case of phosphate release, the S1·HMM amplitude ratio for the pyrene signal change (Fig. 8, *inset*) was somewhat larger than 1.0 over a range of actin concentrations. This suggests that, although the majority of HMM molecules can bind both heads strongly to actin following phosphate release, a small subpopulation can only bind strongly *via* one head. This in turn implies that there is a branch in the myosin V mechanochemical pathway, and this issue will be discussed in the following section.

A Model of Myosin V Processivity—Our results allow us to

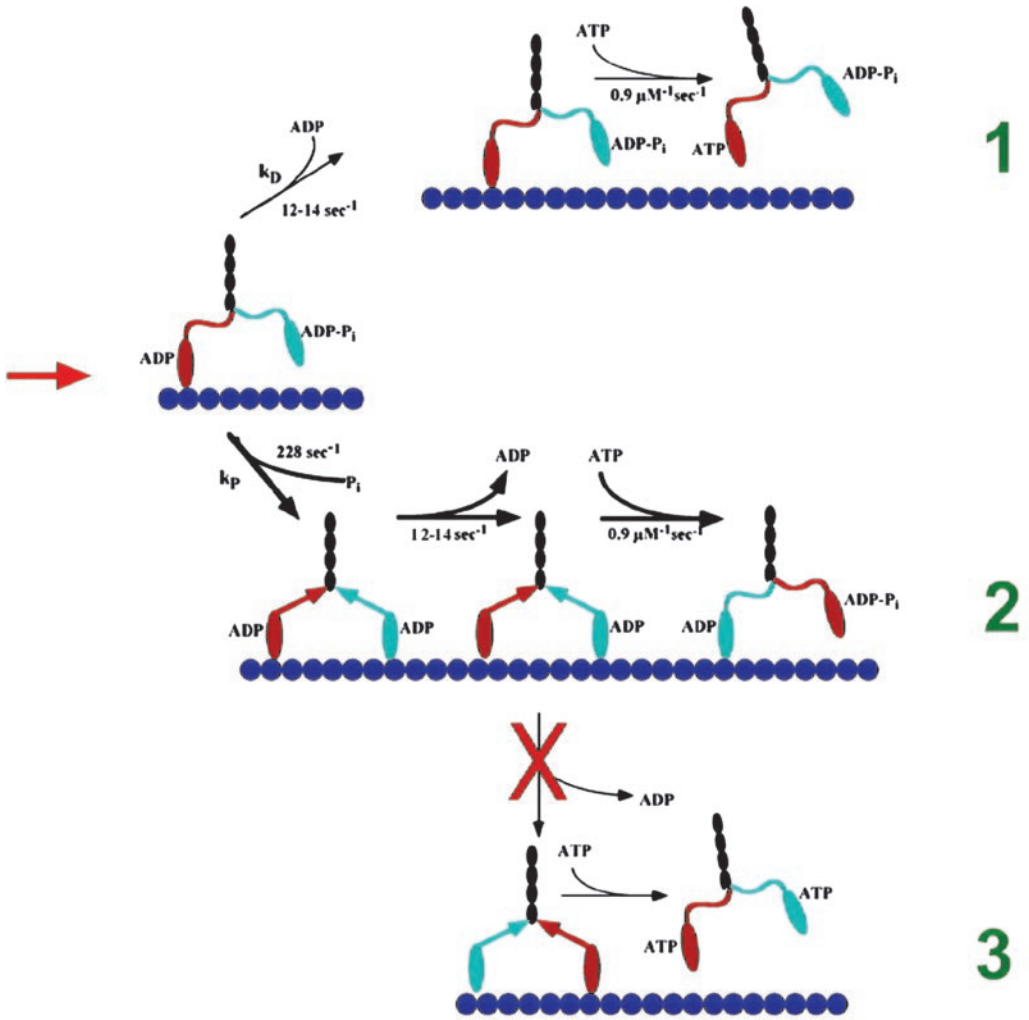

FIG. 10. **Model of myosin V processivity.** The two heads of myosin V are depicted as *ellipses shaded red* and *green* to distinguish them, the lever arms are the correspondingly *shaded linear structures*, and the heptad repeats are *shaded black*. The cycle begins with the species indicated by the *red arrow*, with the rear, ADP-containing head (*red*) strongly bound to actin, and with the forward, ADP-P_i-containing head (*green*) weakly bound or unbound. Three potential reaction schemes are possible, indicated by the *green numbers* in the *right margin*. ADP could be released from the rear head before the forward head could release its phosphate, leading to ATP induced dissociation of the myosin V dimer (scheme **1**). However, scheme **2** is kinetically favored. In this reaction, phosphate is released from the leading head, producing an internally strained complex with ADP in both heads (indicated by the *forward* and *rearward pointing arrows*). Strain-accelerated release of ADP from the rear head is followed by ATP binding and dissociation, which relieves the strain (symbolized by the *serpentine lever arms*). Forward stepping toward the next actin docking site to complete the cycle. Our data also indicate that rearward strain on the forward head blocks ADP release. This feature would be necessary to prevent the doubly-attached, internally strained myosin V intermediate from proceeding down reaction pathway **3** and dissociating prematurely.

propose a new model of myosin V processivity, which is summarized in Fig. 10. We enter the cycle with the species indicated by the *red arrow*, with the ADP-containing head (*red*) strongly bound to actin and the ADP-P_i-containing head (*green*) unbound or weakly bound. At this point, one of two events can occur, indicated by the branching pathway. ADP could be released from the rear head at the unstrained rate constant of 12–16 s^{-1}, and this is indicated by the *lightly shaded arrows* in the reaction pathway marked by the *green number 1*. Given millimolar intracellular ATP concentrations (20–23), this would rapidly lead to dissociation. Alternatively, the second (*green*) head could release its phosphate at 228 s^{-1} (Fig. 7*B*), which would be followed by formation of a species in which both heads are strongly bound (at 47 s^{-1}, Fig. 8). Release of ADP from the rear head followed by ATP binding and forward stepping would complete the cycle, indicated by the pathway marked by the *green number 2*.

Given the rate constants we have measured in this study, we can make testable predictions about myosin V processivity. If phosphate and ADP concentrations are submicromolar, their dissociation from myosin V becomes essentially irreversible. Under these conditions, the probability that a motor will dissociate from its actin track will be directly related to the fraction of molecules that proceed along the upper pathway,

$$\frac{k_D}{k_D + k_P} = \frac{12\ s^{-1}}{12\ s^{-1} + 228\ s^{-1}} = 0.05 \qquad \text{(Eq. 1)}$$

and this would predict a run length of 1/0.05 = 20 steps at 50 mM KCl and 20 °C. This value is approximately half the run length of previous reports (35, 36). However, these studies were performed at higher temperatures (23–30 °C). We note that, although the rate constant for actin-activated phosphate release from S1·ADP·P_i at 20 °C reaches a maximum (Fig. 6*B*), previous experiments at 25 °C showed no such evidence of saturation, and this argues that the kinetics of phosphate release have a strong temperature dependence (9). Therefore, we argue that the longer run lengths reported previously can be entirely consistent with our model when temperature effects are taken into consideration.

Our calculation presumes that weak attachment of the leading head, occurring with rate constant k_p, provides sufficient stability to the doubly attached myosin V to effectively prevent motor dissociation. This assumption is supported by the fact that myosin V binds to actin in the weak binding state with an affinity 10- to 20-fold higher than that for nonprocessive myosins (30). Our model also predicts that, although essentially all of the S1·ADP·P_i motors should release their phosphate during the first enzymatic turnover, a smaller percentage of HMM motors would do so. This is confirmed by the ratio of amplitudes illustrated in the *inset* in Fig. 5.

If the only effect of strain was the acceleration of ADP release from the rear head, myosin V would terminate its processive run after only one or two turnovers. This is illustrated in Fig. 10 by the reaction pathway marked with the *green numbers 2* and *3*. In this reaction mechanism, an intermediate is generated in which the rear head is in rigor and the forward head contains ADP in its active site. If ADP could dissociate from this forward head, ATP would rapidly bind to both heads of this doubly attached species; the motor would follow the reaction pathway indicated by the *green number 3*, and it would dissociate from actin. The only way to prevent this from happening (indicated by the *red X* in the figure) would be to block ADP release from the forward head while the rear head is strongly bound, and presumably, while the system is experiencing internal strain. Our results from this study confirm this prediction (Figs. 2 and 3) and imply that, by dissociating only the trailing head, ATP binding converts the potential energy of mechanical strain to forward motion.

While this manuscript was under review, a single molecule processivity study of myosin V by Baker *et al.* (31) was published. That study put forward a model of processivity that was very different from the one proposed above. The main difference was that the data of Baker *et al.* was consistent with lead head attachment being quite slow (~5/s), thus limiting the rate and degree of processive movement. In contrast, our phosphate release rate suggests that lead head attachment is extremely rapid (>200/s). The possible explanation for this difference can be found in earlier published work, which demonstrates that the equilibrium constant for ATP hydrolysis is increased by >15-fold at 25 °C when an essential light chain occupies the first IQ motif, compared with when CaM occupies this site (32). Although it was pointed out that this would not be significant at physiologic temperature, because the equilibrium constant for hydrolysis greatly increases with temperature, it poses a problem for room temperature assays. A 40-fold decrease in the equilibrium constant for ATP hydrolysis would lower the rate constant for lead head attachment from ~200/s to ~5/s. We suggest that this is the source of discrepancy between our work and that of Baker *et al.* (31).

Another surprising finding of Baker *et al.* was that increasing ADP concentration decreased the degree of processivity. However, this finding is consistent with our results (Fig. 2*B*), which argue that myosin V·ADP is in a dynamic equilibrium between two states: one that binds actin strongly and ADP weakly ($A{\cdot}(M{\cdot}D)^*_{strong}$) and that quenches the fluorescence of pyrene-labeled actin, and one that binds actin with intermediate affinity and ADP strongly ($A{\cdot}(M{\cdot}D)^*_{intermediate}$) and that does not quench pyrene fluorescence. We propose that this equilibrium is strain-dependent; *e.g.* rearward strain on the forward head favors formation of the $A{\cdot}(M{\cdot}D)^*_{intermediate}$ state, while forward strain on the rearward head favors the $A{\cdot}(M{\cdot}D)^*_{strong}$ state. Furthermore, our finding that phosphate release is much faster than the rate of pyrene actin quenching implies that the $A{\cdot}(M{\cdot}D)^*_{intermediate}$ state can be populated under steady-state conditions. Increasing ADP concentrations would then stabilize the rearward head, enhancing the probability that the forward head could dissociate from actin. If ATP then dissociated the rear head, a processive run would terminate.

Comparison to Kinesin—Although the myosin V and kinesin motor domains share some basic structural elements, such as the P loop, switch 1, and switch 2, they share little sequence homology and are generally thought to have come from different motor superfamilies (33). It is thus not surprising; for example, although pre- and post-hydrolytic states are weak and strong binding, respectively, for myosin V, the opposite is true for kinesin (34). Despite these and other differences, however, these two motors share a striking number of similarities in the mechanisms by which they achieve processivity. In both motors, forward strain on the trailing head can accelerate its release for its track by ~2-fold, yet in both motors, this strain-mediated acceleration of nucleotide release is not necessary for the motor to be processive (Ref. 13 and this study). In both motors, rearward strain in the leading head inhibits motor dissociation. For both motors, strain appears to produce these effects by altering the kinetics of nucleotide binding and/or release from the active site. Furthermore, the dominant effect of strain for both is on the leading head, and this effect is the major determinant of how the motor behaves in the steady state. The striking similarities in mechanism between these two unrelated motors suggests that the physiologic demand for processivity shapes a motor's enzymology in a stereotypical way, regardless of its family of origin, and they also support the argument that understanding a motor's enzymology *in vitro* provides valuable insights into its functional role *in vivo*.

REFERENCES

1. Mehta, A. (2001) *J. Cell Sci.* **114,** 1981–1998
2. Goldstein, L. S. B., and Philp, A. V. (1999) *Annu. Rev. Cell Dev. Biol.* **15,** 141–183
3. Forkey, J. N., Quinlan, M. E., Shaw, M. A., Corrie J. E., and Goldman, Y. E. (2003) *Nature* **422,** 399–404
4. Yildiz, A., Forkey, J. N., McKinney, S. A., Ha, T., Goldman, Y. E., and Selvin, P. R. (2003) *Science* **300,** 2061–2065
5. Veigel, C., Wang, F., Bartoo, M. L., Sellers, J. R., and Molloy, J. E. (2001) *Nat. Cell Biol.* **4,** 59–65
6. Vale, R. D. (2003) *J. Cell Biol.* **163,** 445–450
7. Purcell, T. J., Morris, C., Spudich, J. A., and Sweeney, H. L. (2002) *Proc. Natl. Acad. Sci. U. S. A.* **99,** 14159–14164
8. Espindola, F. S., Suter, D. M., Partata, L. B., Cao, T., Wolenski, J. S., Cheney, R. E., King, S. M., and Mooseker, M. S. (2000) *Cell Motil. Cytoskeleton* **47,** 269–281
9. De La Cruz, E. M., Wells, A. L., Rosenfeld, S. S., Ostap, E. M., and Sweeney, H. L. (1999) *Proc. Natl. Acad. Sci. U. S. A.* **96,** 13726–13731
10. Rosenfeld, S. S., Xing, J., Chen, L.-Q., and Sweeney, H. L. (2003) *J. Biol. Chem.* **278,** 27449–27455
11. Rief, M., Rock, R. S., Mehta, A. D., Mooseker, M. S., Cheney, R. E., and Spudich, J. A. (2000) *Proc. Natl. Acad. Sci. U. S. A.*, **97,** 9482–9486
12. De La Cruz, E. M., Ostap, E. M., and Sweeney, H. L. (2001) *J. Biol. Chem.* **276,** 32373–32381
13. Rosenfeld, S. S., Fordyce, P., Jefferson, G. M., King, P. H., and Block, S. M. (2003) *J. Biol. Chem.* **278,** 18550–18556
14. Taylor, E. W. (1991) *J. Biol. Chem.* **266,** 294–302
15. Geeves, M. A., and Holmes, K. C. (1999) *Annu. Rev. Biochem.* **68,** 687–728
16. Holmes, K. C., and Geeves, M. A. (2000) *Philos. Trans. R. Soc. Lond. B Biol. Sci.* **355,** 419–431
17. Coureux, P. D., Wells, A. L., Menetrey, J., Yengo, C. M., Morris, C. A., Sweeney, H. L., and Houdusse, A. (2003) *Nature* **425,** 419–423
18. Yount, R. G., Lawson, D., and Rayment, I. (1995) *Biophys. J.* **68,** 44S–47S
19. Bauer, C. B., Kuhlman, P. A., Bagshaw, C. R., and Rayment, I. (1997) *J. Mol. Biol.* **274,** 394–407
20. Marcussen, M., Overgaard-Hansen, K., and Klenow, H. (1994) *Biochem. Biophys. Acta* **1194,** 197–202
21. Marcussen, M., and Larsen, P. J. (1996) *Cell Motil. Cytoskeleton* **35,** 94–99
22. Nagamatsu, S., Nakamichi, Y., Inoue, N., Inoue, M., Nishino, H., and Sawa, H. (1996) *Biochem. J.* **319,** 477–482
23. Roth, K., and Weiner, M. W. (1991) *Mag. Reson. Med.* **22,** 505–511
24. Hiratsuka, T. (1983) *Biochim. Biophys. Acta* **742,** 496–508
25. Brune, M., Hunter, J. L., Corrie, J. E. T., and Webb, M. R. (1994) *Biochemistry* **33,** 8262–8271
26. Sweeney, H. L., Rosenfeld S. S., Brown, F. Faust, L., Smith, J., Xing, J., Stein L. A., and Sellers, J. R. (1998). *J. Biol. Chem.* **273,** 6262–6270
27. Rosenfeld, S. S., Xing, J., Jefferson, G. M., Cheung, H. C., and King, P. H. (2002) *J. Biol. Chem.* **277,** 36731–36739
28. Walker, M. L., Burgess, S. A., Sellers, J. R., Wang, F., Hammer, J. A., Trinick,

J., and Knight, P. J. (2000) *Nature* **405,** 804–807
29. Cheney, R. E., O'Shea, M. K., Heuser, J. E., Coelho, M. V., Wolenski, J. S., Espreafico, E. M., Forscher, P., Larson, R. E., and Mooseker, M. S. (1993) *Cell* **75,** 13–23
30. Yengo, C. M., De La Cruz, E. M., Safer, D., Ostap, E. M., and Sweeney, H. L. (2002) *Biochemistry* **41,** 8508–8517
31. Baker, J. E., Krementsova, E. B., Kennedy, G. G., Armstrong, A., Trybus, K. M., and Warshaw, D. M. (2004) *Proc. Natl. Acad. Sci. U. S. A.* **101,** 5542–5546
32. De La Cruz, E. M., Wells, A. L., Sweeney, H. L., and Ostap, E. M. (2000) *Biochemistry* **39,** 14196–14202
33. Vale, R. D., and Milligan, R. A. (2000) *Science* **288,** 88–95
34. Rosenfeld, S. S., Rener, B., Correia, J. J., Mayo, M. S., and Cheung, H. C. (1996) *J. Biol. Chem.* **271,** 9473–9482
35. Mehta, A. D., Rock, R. S., Rief, M., Spudich, J. A., Mooseker, M. S., and Cheney, R. E. (1999) *Nature* **400,** 590–593
36. Sakamoto, T., Wang, F., Schmitz, S., Xu, Y., Xu, Q., Molloy, J. E., Veigel, C., and Sellers, J. R. (2003) *J. Biol. Chem.* **278,** 29201–29207